ARMY RESEARCH LABORATORY

Characterization of the Combustion Behavior of Aluminum-Nickel Based Reactive Materials

by Barrie E. Homan, Kevin L. McNesby, John Ritter, Joseph Colburn, and Andrew Brant

ARL-TR-4917   **August 2009**

NOTICES

Disclaimers

The findings in this report are not to be construed as an official Department of the Army position unless so designated by other authorized documents.

Citation of manufacturer's or trade names does not constitute an official endorsement or approval of the use thereof.

Destroy this report when it is no longer needed. Do not return it to the originator.

Army Research Laboratory

Aberdeen Proving Ground, MD 21005

ARL-TR-4917   August 2009

Characterization of the Combustion Behavior of Aluminum-Nickel Based Reactive Materials

Barrie E. Homan, Kevin L. McNesby, John Ritter, Joseph Colburn, and Andrew Brant
Weapons and Material Research Directorate, ARL

REPORT DOCUMENTATION PAGE		*Form Approved* *OMB No. 0704-0188*

Public reporting burden for this collection of information is estimated to average 1 hour per response, including the time for reviewing instructions, searching existing data sources, gathering and maintaining the data needed, and completing and reviewing the collection information. Send comments regarding this burden estimate or any other aspect of this collection of information, including suggestions for reducing the burden, to Department of Defense, Washington Headquarters Services, Directorate for Information Operations and Reports (0704-0188), 1215 Jefferson Davis Highway, Suite 1204, Arlington, VA 22202-4302. Respondents should be aware that notwithstanding any other provision of law, no person shall be subject to any penalty for failing to comply with a collection of information if it does not display a currently valid OMB control number. **PLEASE DO NOT RETURN YOUR FORM TO THE ABOVE ADDRESS.**

1. REPORT DATE *(DD-MM-YYYY)* August 2009	2. REPORT TYPE Final	3. DATES COVERED (From - To) July 2008–July2009
4. TITLE AND SUBTITLE Characterization of the Combustion Behavior of Aluminum-Nickel Based Reactive Materials		5a. CONTRACT NUMBER
		5b. GRANT NUMBER
		5c. PROGRAM ELEMENT NUMBER
6. AUTHOR(S) Barrie E. Homan, Kevin L. McNesby, John Ritter, Joseph Colburn, and Andrew Brant		5d. PROJECT NUMBER
		5e. TASK NUMBER
		5f. WORK UNIT NUMBER
7. PERFORMING ORGANIZATION NAME(S) AND ADDRESS(ES) U.S. Army Research Laboratory ATTN: RDRL-WMB-D Aberdeen Proving Ground, MD 21005		8. PERFORMING ORGANIZATION REPORT NUMBER ARL-TR-4917
9. SPONSORING/MONITORING AGENCY NAME(S) AND ADDRESS(ES)		10. SPONSOR/MONITOR'S ACRONYM(S)
		11. SPONSOR/MONITOR'S REPORT NUMBER(S)
12. DISTRIBUTION/AVAILABILITY STATEMENT Approved for public release; distribution unlimited.		
13. SUPPLEMENTARY NOTES		

14. ABSTRACT

Reactive materials (RM) consist of a wide class of energetic materials that have unique characteristics that can be beneficial to the weapon designer. However, most of the existing information on the behavior of these materials is phenomenological in nature, with little evidence as to the initiation and reaction mechanisms at play. To enable the exploitation of the potential lethality gains, a more fundamental understanding of the initiation and reaction processes was pursued using an array of diagnostic techniques to probe the energy release mechanims. The nickel (Ni)-aluminum (Al) RM system was chosen as the base for the morphology, chemistry, and initiation condition effects studies. Various metals additives were mixed or alloyed with the Al portion of the RM matrix and were subsequently launched by a powder gun into an instrumented chamber to explore the energy release mechanisms. In addition to pressure, high-speed spatial thermometry was used to produce temperature maps that can be directly compared to current modeling efforts. Flash x-ray photography was used to supplement the current suite of high-speed imaging to investigate the effects of surface area generation during impact.

15. SUBJECT TERMS

Reactive materials, aluminum, nickel, combustion

16. SECURITY CLASSIFICATION OF:			17. LIMITATION OF ABSTRACT	18.NUMBER OF PAGES	19a. NAME OF RESPONSIBLE PERSON Barrie E. Homan
a. REPORT Unclassified	b. ABSTRACT Unclassified	c. THIS PAGE Unclassified	UU	24	19b. TELEPHONE NUMBER (*Include area code*) (410) 306-0932

Contents

List of Figures

List of Tables

Acknowledgments

We thank General Science Inc. for producing the samples.

INTENTIONALLY LEFT BLANK.

1. Introduction

The Army has a critical need to fill capability gaps in lethality including incremental nonlethal to lethal effects against personnel and platform, while remaining cognizant of the need for insensitive energetic materials for smart and green munitions. Current classes of energetic materials fall short of such expectations. Reactive materials (RM) are a wide class of energetic materials with unique characteristics that can enable highly lethal munitions for modern tactics like military operations on urban terrain (MOUT) and other applications. These materials are more efficient by potentially replacing the parasitic masses associated with any munition as well as efficiently coupling its energy on target. Unlike conventional materials, the insensitivity of these materials increases the power of the munition without simultaneously increasing the vulnerability of the weapon system. At present, there exists only phenomenological evidence as to the initiation and reaction mechanisms that are at play, making full exploitation of the potential lethality gains difficult. To remedy this situation, an experimental study was implemented with the goal of better understanding the fundamental energy release mechanisms unique to these materials.

The nickel (Ni)-aluminum (Al) RM system was chosen as the family of materials for study under this effort for a variety of reasons. Ni-Al is a simple, nominally bi-metallic system that lends itself to modeling and experimental investigations without the complications of organic chemistry that would result from a binder based system. The energetics of this system, at least from the thermo-equilibrium sense, is straightforward with most of the possible end products being known. This system's performance has also been extensively cataloged (*1, 2*) and the combination of strength and energy should prove useful to munition designers. To understand this system, a matrix of additives and processing techniques were investigated to determine their effects on the initiation and reaction mechanisms.

2. Experimental

The new experimental facility recently installed (*3*) continues to undergo improvements in the techniques and diagnostics used to investigate the energy release structure. The facility centers on the reaction chamber, dubbed the "Green Pig" (figure 1). The Navy's Blue Pig design (*1*), the predecessor of the Green Pig, consisted of a section of industrial pipe with appropriate flanges to seal each end. The Blue Pig used pressure as the metric to determine the performance of the tested reactive materials. Using the Green Pig design, with its transparent face, has allowed for the coupling of advanced spectroscopic and imaging techniques to be applied in situ. As with the Blue Pig, a projectile fabricated from the various candidate materials are sabot-launched from

a 30mm powder gun into the chamber (figure 2). The entrance to the Green Pig has a variable thickness and material plate that the projectile must first penetrate. The remnants of the projectile along with pieces of the plate then travel inside the pig before striking an anvil currently made from rolled homogeneous armor (RHA). Like most other chambers, the Green Pig is capable of measuring the pressure created from the reaction as a function of time. In addition, a suite of diagnostic instruments has been developed and implemented to determine the mechanical state of the projectile (amount of disintegration), timing and quantity of the energy released, and information concerning the chemistry involved in the reaction.

Figure 1. ARL Reactive Material Research Facility's Green Pig.
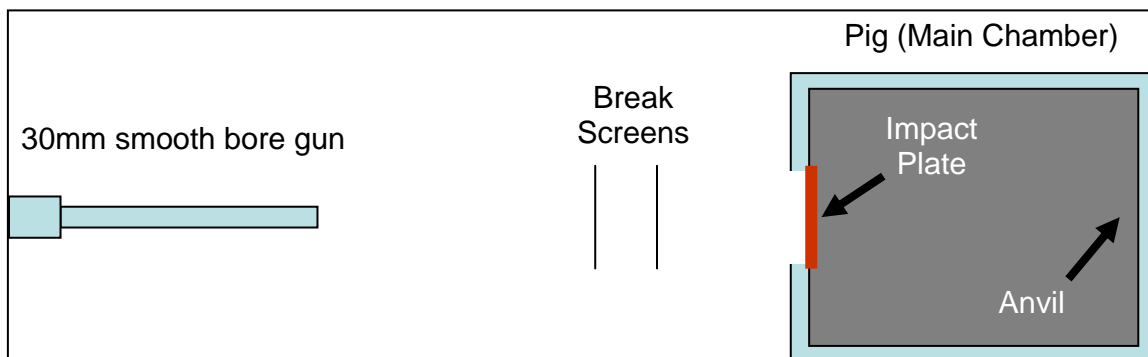

Figure 2. Diagram of the Green Pig Facility.

As imaging of the event is important to discern the state of the material as it transits the chamber from the initial impact plate to the anvil, four visual techniques are employed to investigate various aspects of the event. For an overall picture of the event, a high-speed (HS) camera (Vision Research, Phantom 7.4, B/W) was coupled to two flash bulbs (Megga-Flash PF300) providing overall illumination. Due to the lack of the camera dynamic range exacerbated by the bright emission inherent in the reaction of energetic materials, it is difficult to image non-emitting elements without complete saturation of bright regions resulting from reaction events. A second technique, high brightness (HB) imaging, was incorporated to overcome this difficulty and to probe those regions that are not visible with other techniques during emission. In this

technique (*5*), a high power, short pulse duration (20 ns) laser with a wavelength of 510 nm is synchronized to a HS camera incorporating an appropriate band pass filter. The band pass filter, centered on the 510 nm wavelength with a window of ±5 nm minimizes the emission from the event by admitting only a small section of the continuous spectrum. Using this technique, the amount of broadband light collected from the combustion process is a much smaller percentage than that returning from the laser allowing imaging of regions near the combustion zones. Two new imaging techniques have recently been added to the suite of tools. An Ultra-High-Speed (UHS) camera (Cooke, HSFC) that is capable of up to 8 frames with 1 ns temporal resolution is used to probe the post penetration debris cloud. This technique is also sensitive to emission.

Finally, a four head flash x-ray system (L3 Communications PulseRAD) was added to investigate the fragment size and spatial distribution of the debris cloud as it travels to the anvil. This technique can penetrate the combustion cloud that obscures the particles from the other diagnostics. Two digital x-ray film plates are placed inside the main chamber. The x-rays pass through the 1-in-thick polycarbonate and 1/8-in acrylic windows with little attenuation. The first or left film is near the impact plate and the second or right film is near the anvil. Each of the films has two heads for illuminations (figure 3) so that the two images do not interfere and each head can be individually controlled. Simple optical measurements of the fragments give a good indication of the size of the fragments perpendicular to the x-ray path. Because x-rays are attenuated (*4*) as they pass through a material, the opacity of the image of the fragments can be used to estimate the size of the fragments in the direction of the x-rays.
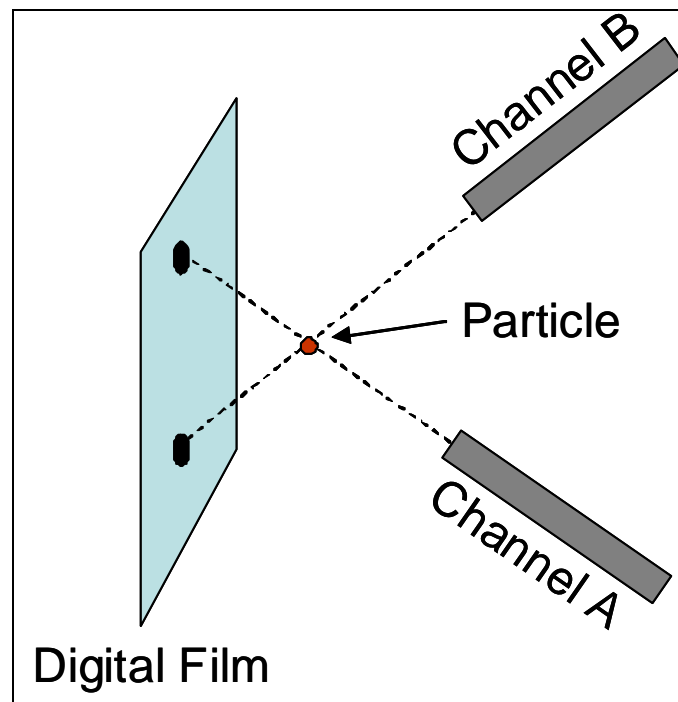

Figure 3. Geometry of the x-ray heads (marked Channels A and B).

As an indication of the amount of energy released during the event, the temperature of the particles is measured using a two-wavelength, HS, spatial pyrometry technique developed in-house (*3*). The heart of the system is two HS cameras (Vision Research Phantom 5.1) operating up to 10,000 fps. Each camera sees the same view through a set of optics that includes a beam splitter. In front of each camera is a narrow band-pass filter (700 or 900 nm and a bandwidth of 10 nm). The movies from each camera are calibrated using a blackbody source at 1000 °C. Using Planck's blackbody relationship (*9*), the temperature map as a function of time can be calculated from the ratio of the intensities recorded from the two cameras. If the wavelengths chosen are in a region of the spectrum not including atomic or molecular gas phase emission, the pyrometry measurement will be unaffected by the local gas temperature. Recording of the broadband spectral signature of the event has shown no such emission in the regions covered by the pyrometer.

3. Results

For this series, a matrix of formulations (table 1) was developed to determine the effects of metal additives on the initiation and combustion properties of the base material. These mixtures of powder ingredients at the desired ratio were isostatically pressed (*6*) under controlled conditions to produce the monolithic samples. Samples produced this way tend to have reduced strength that is directly linked to the porosity. The fraction of the theoretical maximum density (TMD) of a typical sample produced this way is usually low to mid 90%. The metal additives—magnesium (Mg), molybdenum (Mo), copper (Cu), and zinc (Zn)—were initially chosen to study the effects of metal additives on reactivity in the Al-Ni framework. Small amounts of Mg, Mo, and Zn have shown evidence of enhancing performance (*1*), while Cu was considered because of its large effects on the melting point of Al—from 660.4 °C for pure Al to 548.2 °C for 17.2 atomic percent of Cu (*7*). To test the effect of the alloying in energy release, one of the formulations, Al/Ni, was made of a powder that was pre-alloyed.

Table 1. Formulation matrix.

Description	Formulation (% by weight)	Density (g/cc)	Projectile mass (nominal, g)
Base powder	Al/Ni – 31.5/68.5	4.6	7.7
Mo modified	Al/Mo/Ni – 30.3/2.2/67.5	4.9	7.9
Mg modified	Al/Mg/Ni – 28.6/2.4/69.0	4.7	7.6
Cu modified	Al/Cu/Ni – 24.2/11.7/64.1	5.2	8.6
Mg/Zn modified	Al/Mg/Zn/Ni 23.68/2.01/9.38/64.93	4.89	8.2
Steel	N/A	7.8 nom.	11.4
Al billet	N/A	2.6 nom.	4.0

4

The sabot/RM projectiles were launched from a 30mm smooth bore powder gun at an average velocity of 1615 ±39 m/s. The sabot was a two-piece design that is stripped from the flight path after muzzle exit. The velocity was measured by three break screens with the last screen mounted to the front of the pig and acting as the time zero fiduciary mark. When the sample collides with the impact plate on the front of the main chamber, there appears some emission from the interaction of the sample. The main focus of the pre-chamber was to quantify this energy release to so that all energy from the interaction is being tracked. Measurements of the pressure inside the pre-chamber showed, being related to energy release, that a negligible amount of reaction is taking place outside the main chamber. Although the gun propellant charge was held constant at maximum practical loading density, small variations in the mass of the projectile package and variations on the propellant combustion event led to variable terminal velocity. In addition, a more precise timing of the sample arrival, critical for some of the diagnostics, was needed because the variable delivered velocity, although small, led to mistiming. For these reasons, the pre-chamber was removed and the break screen used for the time fiduciary was placed on the main chamber plate for some of the later tests.

The next encounter is with the impact plate and this can be varied in thickness as well as material. For the results discussed here, the impact plate parameters (mild steel of 1/16 in [0.158 cm] thick) were kept constant. From the interaction with the impact plate, the projectile enters the chamber in some degree of pulverization depending on the initial strength of the material. Inside the chamber a second plate of RHA steel 2 in thick acted as an anvil.

The morphology of the debris cloud depends on the original strength of the projectile material and an indication of the particle size and shapes can be obtained by flash x-rays. Steel, being the strongest material tested to date, mostly broke up into large pieces (figure 4). The penetrated steel plate is off the image to the left of the picture and the anvil is to the right. The height of the debris cloud from the bottom of the images is immaterial because it is only affected by the particular shot geometry. The projectile target grouping is on the order of 3–4 in and this affects where on the film plate the images are captured. The center of mass for each of the images is in a ballistic line through the pig. Because the spatial scales are equal for each individual set of images, it is clear that the fragments are dispersing as they travel down range.

Figure 4. Steel projectile fragment progression; anvil is to the right.

The next strongest material tested was Al billet. The fragments from the impact are still large (figure 5) but appear more flake-like than the steel. This is evidenced by the large but nearly transparent pieces shown traveling behind the main fragment. This main fragment, at the front edge of the cloud, could consist of the piece impact plate knocked out by the projectile only or could also contain a fragment of aluminum in a cup-shaped impact plate fragment.
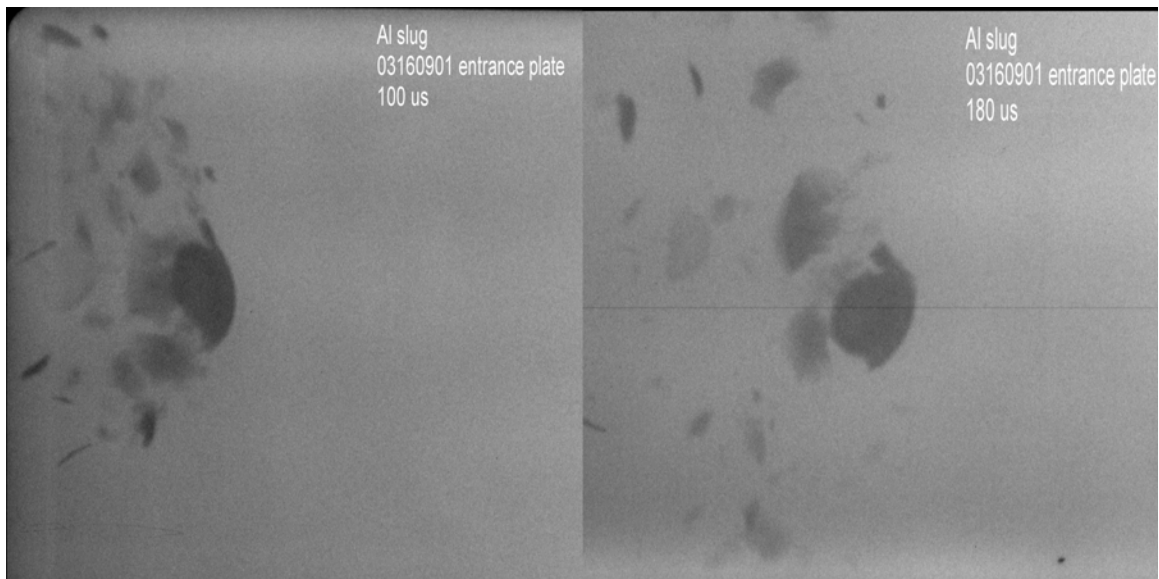

Figure 5. Al billet sample.

For the baseline reactive material (Al/Ni), the morphology (figure 6) of the debris cloud is markedly different than either the steel or Al billet samples. There is clear evidence that the sample is breaking up into much smaller particles with some flake-like materials, possibly the remnants of the steel plate. The cloud is quickly acquiring the expected Mach cone shape. The shape of the front edge of the particle cloud is an indication as to the uniformity and predominant sizes of the debris.

Figure 6. Al/Ni base sample.

When copper was the additive (figure 7), almost complete breakup of the original projectile happens early on in the event. The particles are already showing signs of size sorting with the finer particles trailing due to aerodynamic drag considerations. Similar behavior is seen when the additive is changed to Mg/Zn (figure 8).
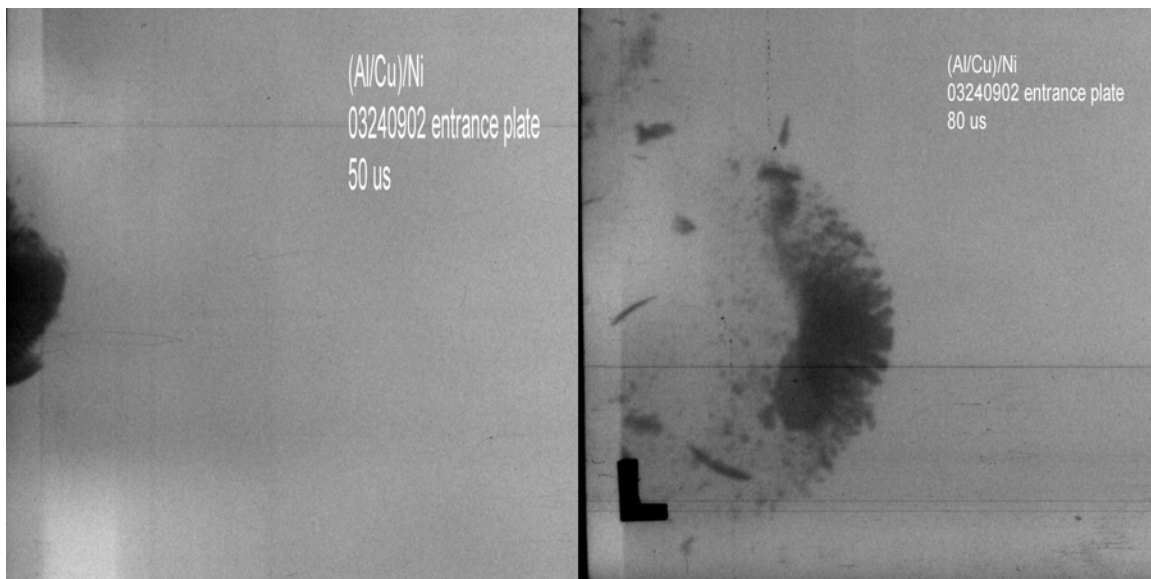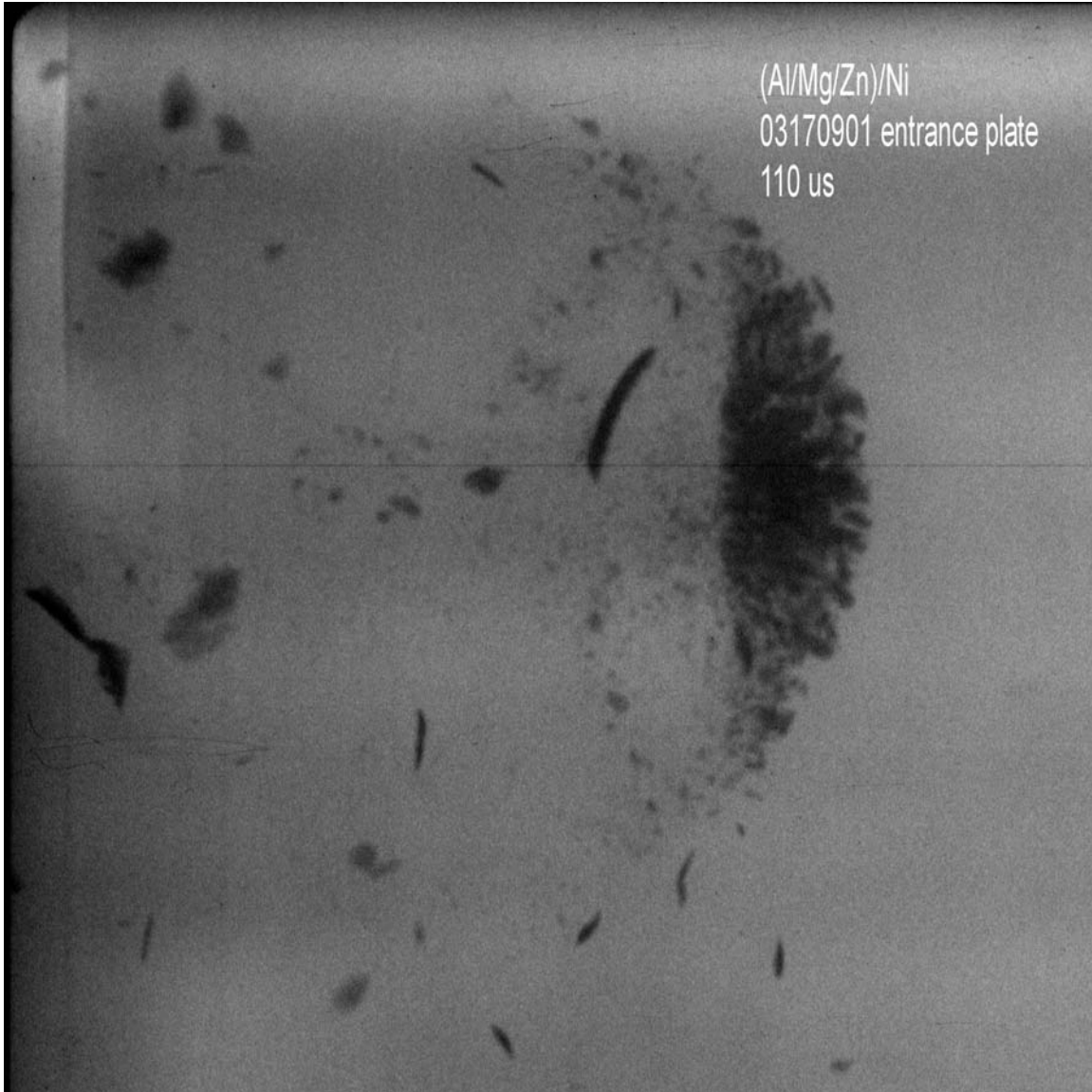

Figure 7. (Al/Cu)/Ni sample.

Figure 8. (Al/Mg/Zn)/Ni sample.

In figure 9, a series of HS images from a typical experiment is shown. The sample in this case includes the addition of Cu. The HS camera frequency varied, with this particular sequence taken at 17,021 fps or 59 μs between frames. The perforation of the steel plate is just beginning at –24 μs (figure 10, right). The camera has a temporal uncertainty of ±½ frame or ±29 μs for this case. There is some reaction taking place initiated by the penetration as seen from time 35 μs on (figure 9). However, there is a significant portion of the sample that has not been ignited, shown by the other techniques discussed below where it is seen leading the flame contact surface. At 505 μs, these particles are just about to hit the anvil. The next frame, 563 μs into the event, these particles ignite and the combustion wave begins to spread back into the chamber. Using the known distances and times, the fragment cloud is traveling at approximately 1,200 m/s or a 20–25% reduction in velocity from the effects of penetration and aerodynamic drag.
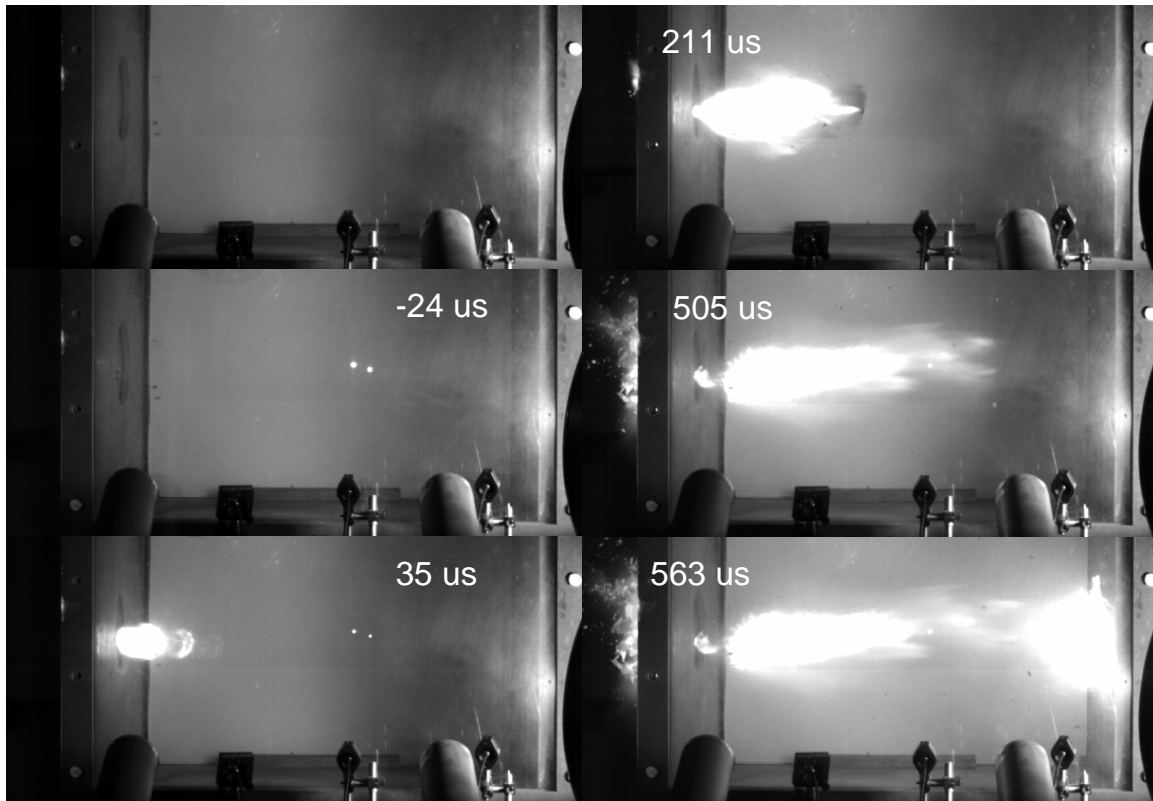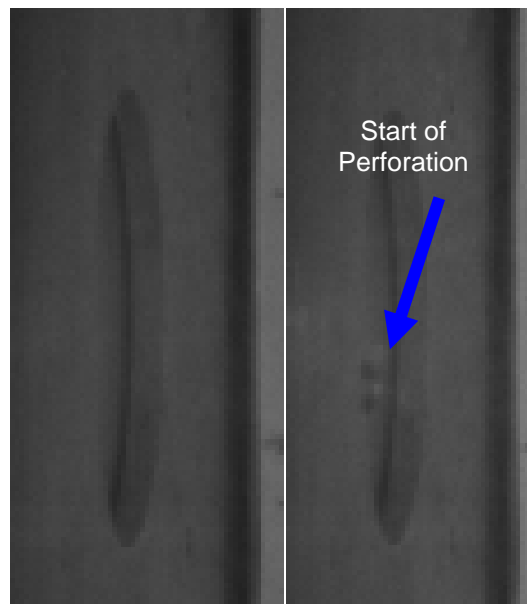
Figure 9. HS imaging of Al-Cu-Ni sample.

Figure 10. Start of perforation of impact plate.

Because the un-reacted particles are difficult to see in conventional imaging, HB imaging complemented the HS technique. A series of images from this technique is shown in figure 11. The fragments in the cloud are more easily distinguished in these images as compared to the HS.

9

In particular, it is easy to see that the particles are distributed throughout the path of the cloud with the largest pieces out front. These particles become the fuel for the combustion wave that progresses back into the chamber after initiation at the anvil. As the RM particle cloud enters the field of view (FOV) from the left, a typical mushroom shape of debris is clearly discernable with accompanying bow shock being imaged. The particles are being sorted by mass due to aerodynamic drag with the heavier particle retaining the highest velocity due to inertia.
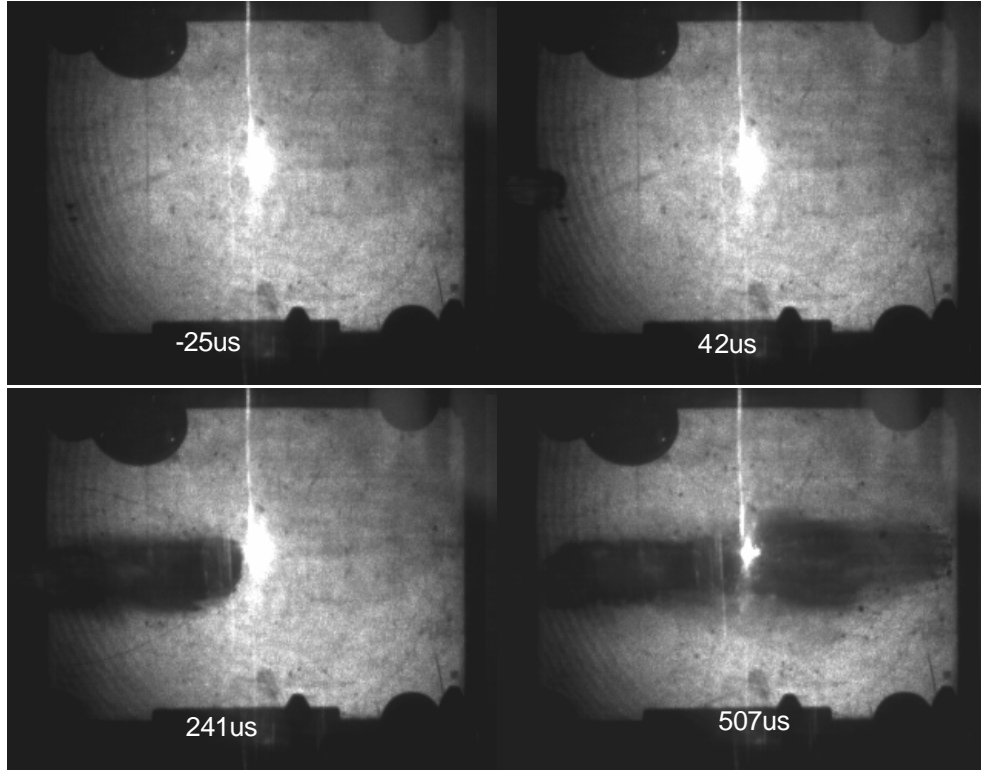

Figure 11. HB imaging of Al-CU-Ni test sample.

Complementing the visual imaging techniques is the two-color pyrometry. In figure 12, the thermal maps at t = 1.4 ms for three formulations given in table 1—Al/Ni, Al/Cu/Ni, and pre-alloyed Al/Ni—are compared. The images on the left in figure 12 show the thermal maps where the sample entered the chamber from the left and has impacted the anvil on the right. On the right side of the figure, a histogram of the temperatures seen in the maps on the left are tabulated. These histograms assist in determining the most prevalent temperatures as well as giving an indication of the breadth of temperatures occurring inside the chamber. In each of the temperature maps of figure 12, there is a trail of energy release from the initial impact as evidenced by the narrow jet from the left side of the pictures. At this early time, there appears little quantitative difference between the pre-alloyed material and its standard powder mixture counterpart. The addition of Cu at the expense of Al does produce a significantly hotter region at

10

the front of the combustion wave. This can be seen from the temperature maps. The histogram for this formulation confirms that the front edge is burning 300–400 °C hotter than the bulk region pointing to the possibility that two processes are occurring.
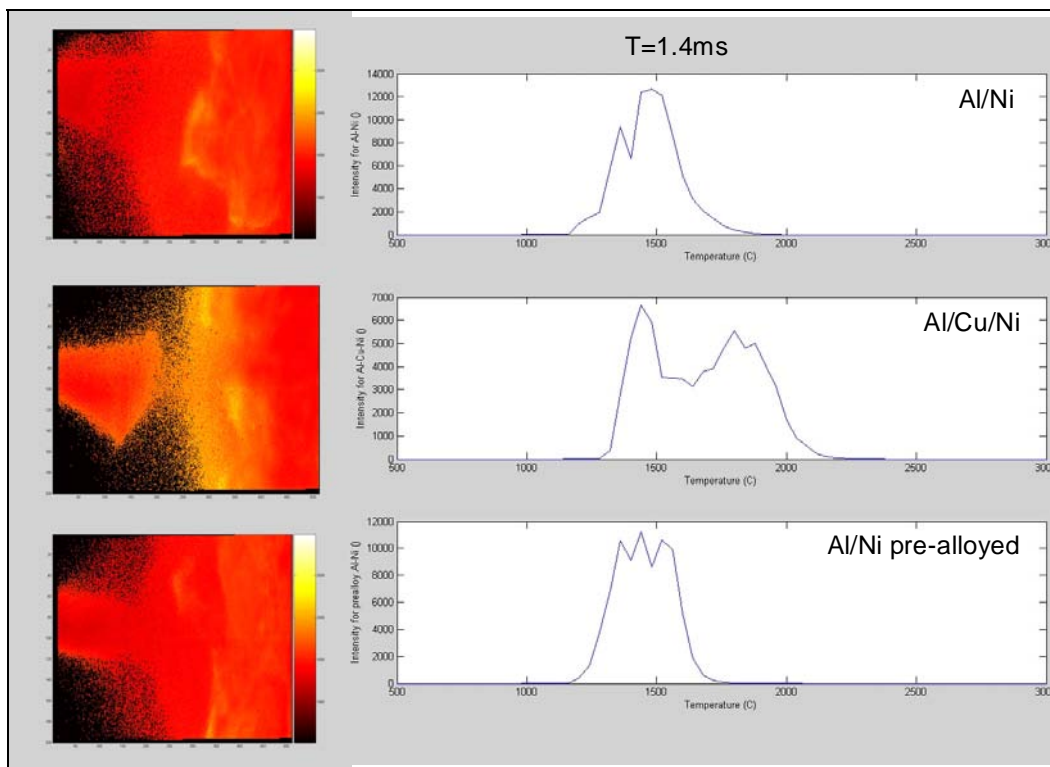

Figure 12. Thermal maps at 1.4 ms.

Comparisons of some of the other formulations are shown in figure 13. In these series of tests, the Mo and Mg formulations have similar temperature profiles with a clear bi-distribution of temperatures with the cooler region being on the front edge of the combustion wave, on the left of the fireball. This behavior would be expected in a presence of an expansion wave. The notable exception is the Cu-modified material. As in figure 12, the Cu produced an increased temperature region at the front of the combustion wave. Later on in the event (figure 14), clear evidence of cooling has taken place as the average temperature has dropped 300 to 500 °C. The standard pressed powder mix of Al and Ni is now in its cooling only phase with little evidence of continuing combustion. The pre-alloyed materials have some regions that show increased temperature in the region of the anvil (on the right). The Cu is still exhibiting a higher average temperature than either of the other samples.
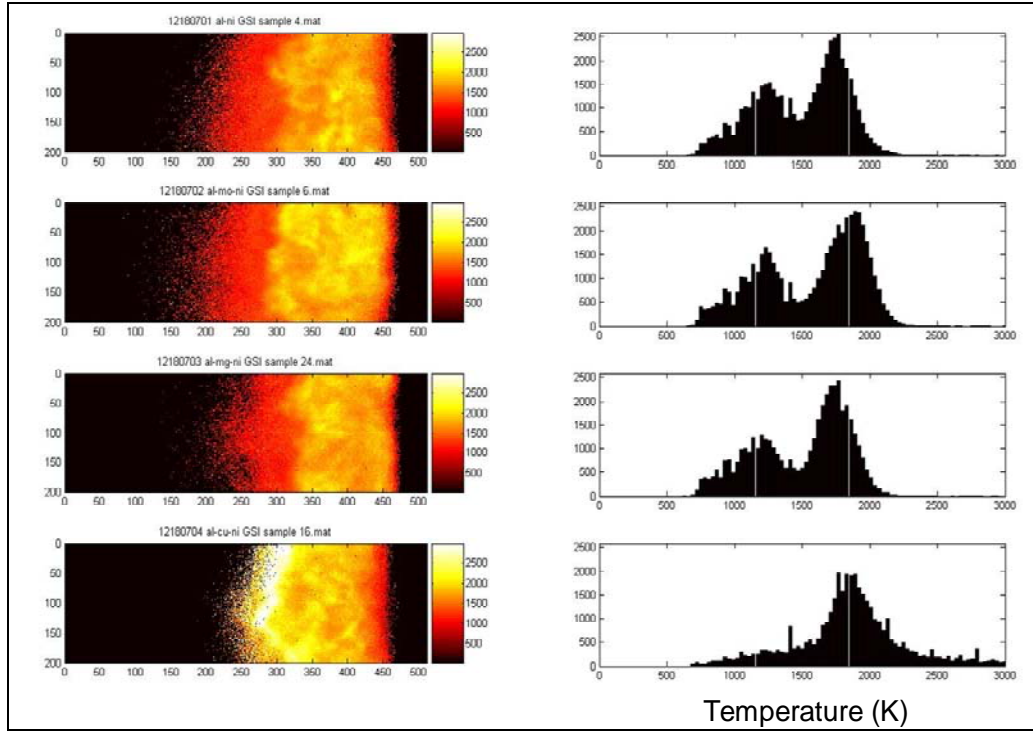
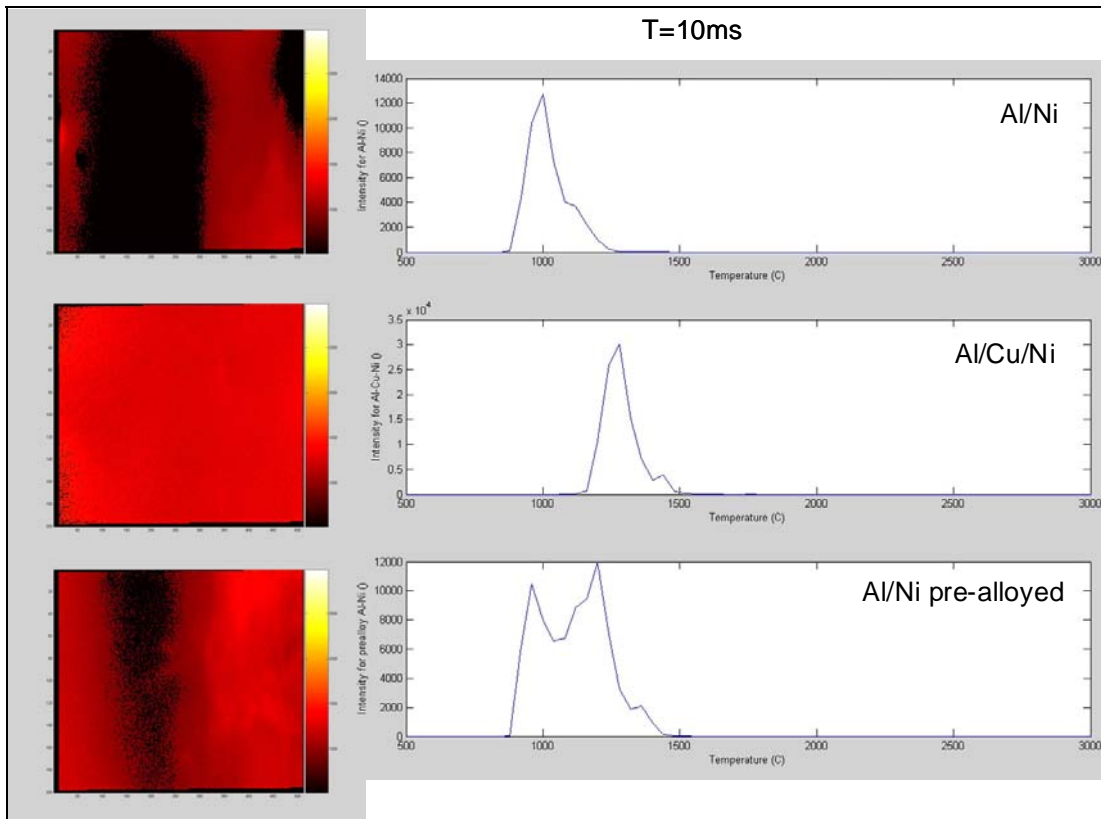Figure 13. Thermal maps of other formulations at T = 1.4 ms.

Figure 14. Temperature maps at T = 10 ms.

4. Conclusions

In this effort, we investigated a variety of formulations based on the Al-Ni family of RM. We applied a suite of diagnostic techniques to investigate the initiation and combustion behavior of these materials. The sequence of events started with the pulverization of the RM by penetration through the impact plate. Although some of the chemical energy was released in this interaction, the majority was preserved as the debris field continued into the chamber. The amount of pulverization of the original projectile depended on the strength of the formulations with highly consolidated samples (steel and Al) breaking into a smaller number of larger pieces and the pressed powder samples being more friable. As the material traveled, the particles tended to sort by size due to aerodynamic forces. The heaviest particles were the first to initiate on impact with the anvil, producing a combustion wave that traveled back through the finer particles suspended throughout the chamber. The addition of different metals to the formulation affected the combustion process in different ways. The addition of Mg at this concentration had little effect. The Mo-modified material showed slightly higher temperatures early on, with that difference decreasing further into the event. The addition of Cu, however, showed a marked increase in initial temperature as well as evidence of continued reaction further into the chamber.

5. References

1. Ames, R. Naval Surface Warfare Center Program Summary, XB-NSWCDD/VA, Naval Surface Warfare Center: Dahlgren, VA, 2003.

2. Richards, D. W.; Kramer, M. P.; Wilson, W. H. *Development and Characterization of Advanced Energetic Composite (AEC) Reactive Materials;* AFRL-MN-EG-TR-2004-7013; Air Force Research Laboratory: Wright-Patterson AFB, OH, 2003.

3. Homan, B. E.; McNesby, K. L.; Pandey, R.; Ritter, J.; Colburn, J.; Brant, A. *Fundamental Mechanism of Energy Release in Reactive Materials*; ARL-TR-4524; U.S. Army Research Laboratory: Aberdeen Proving Ground, MD, 2008.

4. Hubbell, J. H. *Bibliography of Photon Total Cross Section (Attenuation Coefficient) Measurement 10 eV to 13.5 eV, 1907–1993*; NISTIR 5437; National Institute of Standards and Technology: Gaithersburg, MD, 1994.

5. McNesby, K. L.; Homan, B. E. *Real Time Optical Measurements for Improved Understanding of Enhanced Blast Materials*; ARL-TR-3483; U.S. Army Research Laboratory: Aberdeen Proving Ground, MD, 2005.

6. McNesby, K. L.; Homan, B. E.; Piehler, T. N.; Lottero, R. E. *Spectroscopic Measurements of Fireballs Produced by Enhanced Blast Explosives*; ARL-TR-3318; U.S. Army Research Laboratory: Aberdeen Proving Ground, MD, 2004.

7. General Sciences Inc. Final Report on Reactive Materials as Lethality Enhancers, 2006.

8. SGTE alloy database, Center for Research in Computational Thermochemistry. http://www.crct.polymtl.ca/ (accessed 2009).

9. McNesby, K. L.; Homan, B. E.; Lottero, R. E. *High Brightness Imaging for Real Time Measurement of Shock, Particle, and Combustion Fronts Produced by Enhanced Blast Explosives*; ARL-TR-3411; U.S. Army Research Laboratory: Aberdeen Proving Ground, MD, 2005.

10. Möller, K. D. *Optics*; University Sciences Books: Mill Valley, CA, 1988.

List of Symbols, Abbreviations, and Acronyms

Al	aluminum
Cu	copper
FOV	field of view
HB	high brightness
HS	high speed
Mg	magnesium
Mo	molybdenum
MOUT	military operations on urban terrain
Ni	nickel
RM	reactive materials
RHA	rolled homogeneous armor
TMD	theoretical maximum density
UHS	Ultra-High-Speed
Zn	zinc

1 DEFENSE TECHNICAL
   (PDF INFORMATION CTR
ONLY) DTIC OCA
       8725 JOHN J KINGMAN RD
       STE 0944
       FORT BELVOIR VA 22060-6218

1 DIRECTOR
   US ARMY RESEARCH LAB
   IMNE ALC HRR
   2800 POWDER MILL RD
   ADELPHI MD 20783-1197

1 DIRECTOR
   US ARMY RESEARCH LAB
   RDRL CIM L TECHL LIB
   2800 POWDER MILL RD
   ADELPHI MD 20783-1197

1 DIRECTOR
   US ARMY RESEARCH LAB
   RDRL CIM P TECH PUBS
   2800 POWDER MILL RD
   ADELPHI MD 20783-1197

1 DIR USARL
   RDRL ROP TECH LIB
   PO BOX 12211
   RESEARCH TRIANGLE PARK NC
   27709-2211

1 US ARMY
   PEO AMMO PMCAS
   SFAE AMO CAS
   J IRIZARRY
   BLDG 171A
   PICATINNY ARSENAL NJ 07806-5000

1 COMMANDER
   RADFORD ARMY AMMO PLANT
   SMCAR QA HI LIB
   RADFORD VA 244141-0298

1 DIR BENET WEAPONS LAB
   TECH LIB
   WATERVLIET NY 12189-4000

1 CDR NAVAL RSRCH LAB
   TECH LIB
   WASHINGTON DC 20375-1972

2 OFFICE OF NAVAL RSRCH
   C BEDFORD
   B ALMQUIST
   875 N RANDOLPH ST RM 653
   ARLINGTON VA 22203-1927

3 CDR
   NAVAL SURFACE WARFARE CTR
   CODE 910
   R LEE
   S KIM
   R JOUET
   101 STRAUSS AVE
   INDIAN HEAD MD 20640

1 GENERAL SCIENCE INCOPORATED
   A ROZANSKI
   205 SCHOOLHOUSE ROAD
   SOUDERTON PA 18964

ABERDEEN PROVING GROUND

1 DIR USARL
   RDRL CIM G (BLDG 4600)

15 DIR USARL
    RDRL WMB D
     C CANDLAND
     M ZOLTOWSKI
     R A BEYER
     A L BRANT
     J COLBURN
     B E HOMAN
     K L MCNESBY
     J RITTER
     R C SAUSA
    RDRL WMT C
     M FERMEN-COKER
     R SUMMERS
    RDRL WMT B
     B MCANDREW
     R EHLERS
    RDRL WMM C
     V CHAMPAGNE
     M TREXLER

TOTAL: 31 (1 ELEC, 30 HCs)